Geophysical Journal International

Geophys. J. Int. (2016) **204,** 798–812 doi: 10.1093/gji/ggv486

GJI Geomagnetism, rock magnetism and palaeomagnetism

How fast was the Matuyama–Brunhes geomagnetic reversal? A new subcentennial record from the Sulmona Basin, central Italy

Leonardo Sagnotti,[1] Biagio Giaccio,[2] Joseph C. Liddicoat,[3] Sebastien Nomade,[4] Paul R. Renne,[5,6] Giancarlo Scardia[7] and Courtney J. Sprain[5,6]

[1] *Istituto Nazionale di Geofisica e Vulcanologia, I-*00143*, Roma, Italy. E-mail: leonardo.sagnotti@ingv.it*
[2] *Istituto di Geologia Ambientale e Geoingegneria, CNR, I-*00015 *Monterotondo, Rome, Italy*
[3] *Barnard College, Columbia University, New York, NY* 10027*, USA*
[4] *Laboratoire des sciences du climat et de l'environnement, UMR*8212*, IPSL, CEA/CNRS/UVSQ et Université Paris–Saclay,Gif-Sur-Yvette, F-*91190*, France*
[5] *Berkeley Geochronology Center, Berkeley, California, CA* 94709*, USA*
[6] *Department of Earth and Planetary Science, University of California, Berkeley, CA* 94709*, USA*
[7] *Instituto de Geociências e Ciências Exatas, Universidade Estadual Paulista, Rio Claro–SP,* 13506-900*, Brazil*

Accepted 2015 November 5. Received 2015 November 5; in original form 2015 July 8

SUMMARY

A recent study of the Matuyama–Brunhes (M-B) geomagnetic field reversal recorded in exposed lacustrine sediments from the Sulmona Basin (Italy) provided a continuous, high-resolution record indicating that the reversal of the field direction at the terminus of the M-B boundary (MBB) occurred in less than a century, about 786 ka ago. In the sediment, thin (4–6 cm) remagnetized horizons were recognized above two distinct tephra layers—SUL2-19 and SUL2-20—that occur ∼25 and ∼35 cm below the MBB, respectively. Also, a faint, millimetre-thick tephra (SUL2-18) occurs 2–3 cm above the MBB. With the aim of improving the temporal resolution of the previous Sulmona MBB record and understanding the possible influence of cryptotephra on the M-B record in the Sulmona Basin, we performed more detailed sampling and analyses of overlapping standard and smaller samples from a 50 cm-long block that spans the MBB. The new data indicate that (i) the MBB is even sharper than previously reported and occurs ∼2.5 cm below tephra SUL2-18, in agreement with the previous study; (ii) the MBB coincides with the rise of an intensity peak of the natural remanent magnetization (NRM) intensity, which extends across SUL2-18; (iii) except for a 2-cm-thick interval just above tephra SUL2-18, the rock magnetic parameters (k, ARM, M_r, M_s, B_c, B_{cr}) indicate exactly the same magnetic mineralogy throughout the sampled sequence. We conclude that either SUL2-18 resulted in the remagnetization of an interval of about 6 cm (i.e. during the NRM intensity peak spanning ∼260 ± 110 yr, according to the estimated local sedimentation rate), and thus the detailed MBB record is lost because it is overprinted, or the MBB is well recorded, occurred abruptly about 2.5 cm below SUL2-18 and lasted less than 13 ± 6 yr. Both hypotheses challenge our understanding of the geomagnetic field behaviour during a polarity transition and/or of the NRM acquisition process in the Sulmona lacustrine sediment.

Key words: Palaeomagnetic secular variation; Rapid time variations; Reversals: process, time scale, magnetostratigraphy; Rock and mineral magnetism.

INTRODUCTION

The stochastic directional change of the Earth's magnetic field is one of the most striking phenomena of its intrinsic instability (Biggin *et al.* 2012). Our knowledge of the dynamics and tempo of this complex phenomenon is a requirement for our comprehension of the underlying physical processes in the Earth's outer core. This knowledge currently rests on records of geomagnetic field reversals preserved in lava flows or sedimentary successions (Coe and Glen 2004). Lava flows preserve discontinuous 'spot readings' of the geomagnetic field, making the assessment of the tempo of polarity reversals rather difficult and ambiguous. On the other hand, sedimentary sequences provide continuous palaeomagnetic records making these temporal series potentially more suitable for addressing the issue. However, the record in sediments is not completely understood and can be delayed by post-depositional remanent magnetization (pDRM) processes, including the alignment to the ambient magnetic field and the immobilization (lock-in) of particle

magnetic moments due to dewatering and compaction (Verosub 1977). Such effects may result in the smoothing of a sharp geomagnetic signal and a possible stratigraphic downward shift of recorded geomagnetic features (lock-in depth), according to a variable lock-in function (Hyodo 1984; Roberts & Winklhofer 2004; Sagnotti *et al.* 2005; Liu *et al.* 2008; Suganuma *et al.* 2011; Mellstrom *et al.* 2015). On the whole, the reliability and suitability of sedimentary archives for evaluating the tempo of the geomagnetic reversal depend on specific characteristics and properties of the sediments, which include (i) integrity and continuity of the stratigraphic succession; (ii) quality of the palaeomagnetic properties; (iii) homogeneity of the rock magnetic properties and of the magnetic mineralogy and (iv) quality of the chronological constraints.

The recent palaeomagnetic and rock magnetic study of the lacustrine sediments exposed in the Sulmona Basin in the central Apennines (Italy) has shown a high potential for addressing these issues (Sagnotti *et al.* 2014). In the basin, the polarity transit of the Matuyama–Brunhes (M-B) geomagnetic reversal is recorded ∼2–3 cm below a cryptotephra (SUL2-18) as a very fast event, which according to the $^{40}Ar/^{39}Ar$ chronological framework occurred within less than a century. However, it was also recognized that thin intervals (4–6 cm thick) of lacustrine sediments on top of two major tephra layers (SUL2-19 and SUL2-20) deposited during the Matuyama Chron were remagnetized after the M-B reversal, resulting in apparent sharp transitions to normal palaeomagnetic directions before the actual M-B polarity transition (Sagnotti *et al.* 2014).

With the aim of increasing the temporal resolution of the palaeomagnetic record bracketing the M-B reversal and to better understand the potential influence of cryptotephra SUL2-18 on the fidelity of this record, we resampled the Sulmona lacustrine sediments containing the M-B boundary (MBB). To achieve this objective, we performed an ultrahigh-resolution analysis of the palaeomagnetic and rock magnetic properties in a 50-cm-thick interval spanning the MBB and the SUL2-18 cryptotephra. The results refine previous inferences about the actual duration of the Virtual Geomagnetic Pole (VGP) transit and the involved sediment remanence acquisition processes.

STRATIGRAPHIC, CHRONOLOGICAL AND PALAEOMAGNETIC SETTINGS

The Quaternary sedimentary fill of the Sulmona Basin, central Italy (Fig. 1), is composed of three main unconformity-bounded fluvial-lacustrine units (SUL6, SUL5 and SUL4-3) spanning discontinuously the last 820 kyr (Giaccio et al. 2013; Galli *et* al. 2015; Regattieri *et al.* 2015). Our study focused on an interval ∼50 cm thick between the depths of ∼41.6 and ∼42.1 m of the lowermost unit (SUL6) (Giaccio *et al.* 2015). By tephrochronology and the $^{40}Ar/^{39}Ar$ dating method, SUL6 spans ∼820–530 ka (Giaccio *et al.* 2013) and contains the M-B geomagnetic reversal (Giaccio *et al.* 2013; Sagnotti *et al.* 2014; Fig. 2). The lithology of the SUL6 unit consists of massive to faintly laminated white marls with a high concentration of biogenic micrite, which indicates continuous sedimentation in a relatively deep lake environment (Giaccio *et al.* 2015). The continuity of sedimentation is also indicated by the smooth variation in $\delta^{18}O$ through this interval (Giaccio *et al.* 2015) and by the homogeneity of its macroscopic and the fine-scale stratigraphic features (e.g. tephra order and thickness of the interbedded lake sediments, small lithological and colour variability), that can be laterally traced through the whole basin. This is also confirmed by $^{40}Ar/^{39}Ar$ dating of several tephra layers in the SUL6 unit that allows for a reliable estimation of the sedimentation rate and implies a relatively straightforward accumulation history (Sagnotti *et al.* 2014; Giaccio *et al.* 2015). The M-B reversal record has been studied in detail in the exposed section named 'Horseshoe' (HS) (Fig. 1), which extends between tephra layers SUL2-16 and SUL2-22. According to the most recent Bayesian age model produced by an improved $^{40}Ar/^{39}Ar$ geochronology (Giaccio *et al.* 2015), the HS section is constrained between 791.5 ± 2.5 and 784.9 ± 2.5 ka (95 per cent-confidence) (Fig. 2), giving an average sedimentation rate of ∼0.35 mm yr^{-1}.

At the HS section (Figs 1 and 2), the terminus of the M-B polarity transition was found to be a very sharp polarity flip with no intermediate palaeomagnetic directions at 41.85 m of the composite SUL6 section. The change from reverse to normal polarity occurs between two consecutive palaeomagnetic cubes of 2 cm on a side (Sagnotti *et al.* 2014). The cryptotephra SUL2-18, which is a millimetre-thick dark and discontinuous layer, occurs at 41.82 m, 2–3 cm above the M-B polarity transition (Fig. 2). SUL2-18 is associated with a distinct positive peak in the magnetic susceptibility and NRM (Fig. 2). Even more pronounced are the peaks of the ∼5-cm-thick remagnetized interval at the top of the thicker and coarser-grained tephra layers SUL2-19 and SUL2-20, at 42.08 and 42.18 m, respectively (Fig. 2).

SAMPLING AND METHODS

In 2014 December, we resampled the HS section at a distance of ∼50 m (Latitude 42°09′04″N–Longitude 13°49′17″E) from the previously sampled section. Using tephra SUL2-19 as a marker horizon, we collected a single 50-cm-thick block of sediment for ultrahigh-resolution palaeomagnetic and rock magnetic measurements (Fig. 3a). In the laboratory, the block was subdivided into three partially overlapping columns (Fig. 3b), from which we obtained partially overlapping cubes of 2 cm on a side, or smaller parallelepipeds, as shown in Figs 3(c)–(e). This procedure allowed us to increase the sampling resolution, 2–6 times higher (from ∼1 cm to ∼0.3 cm) than that formerly achieved (∼2 cm; Sagnotti *et al.* 2014). In this study, we used a depth scale relative to the base of tephra SUL2-19 (42.08 m in the composite section), set as the origin of the analysed section, which is an unambiguous stratigraphic marker that is easy to identify in the field (Fig. 3a). For comparison, the depths used in the previous study are also reported and shown in Fig. 2. All samples are identified by the distance of their centre from the base of tephra SUL2-19.

All of the samples were measured in the palaeomagnetic laboratory of the *Istituto Nazionale di Geofisica e Vulcanologia* in Rome. We first measured the magnetic susceptibility, normalized by unit volume, using a multifunction kappabridge (AGICO MFK1-FA). Then we measured the natural remanent magnetization (NRM) of all specimens on a small access (45 mm diameter) automated pass through '2 G Enterprises' DC 755 superconducting rock magnetometer (SRM) equipped with Superconducting Quantum Interference Device (SQUID) sensors, housed in a Lodestar Magnetics shielded room. The SRM is equipped with in-line orthogonal alternating field (AF) demagnetization coils, with optional application of a single-axis direct current (dc) field for production of an anhysteretic remanent magnetization (ARM). The NRM was then AF demagnetized using the same protocol as Sagnotti *et al.* (2014), in 13 steps up to 100 mT. After AF demagnetization of the NRM, an ARM was produced by simultaneous application of an AF peak of

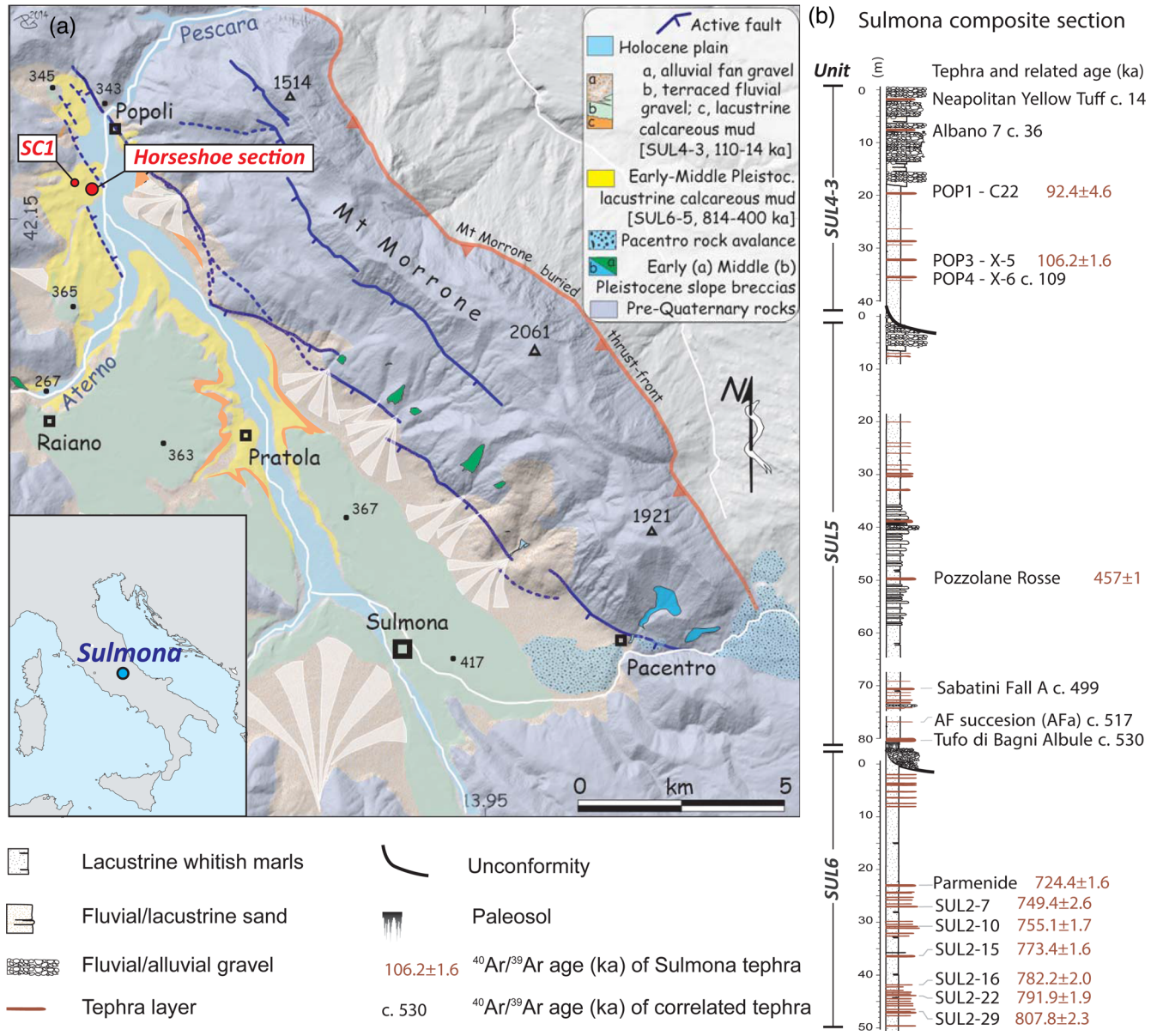

Figure 1. Geological and stratigraphic framework of the Horseshoe section. (a) Simplified geological map of the Sulmona Basin (from Galli *et al.* 2015), the location of the core SC1 is also shown; (b) composite stratigraphic section of the three main unconformity bounded fluvio-lacustrine units with related $^{40}Ar/^{39}Ar$ and tephrostratigraphic chronological constraints (from Giaccio *et al.* 2012, 2013; Sagnotti *et al.* 2014; Galli *et al.* 2015; Giaccio *et al.* 2015; Regattieri *et al.* 2015).

100 mT and a dc bias field of 0.05 mT, while the samples were translated through the AF and dc coil system at a speed of 10 cm s^{-1}, the lowest speed allowed by the software controlling the measurements. The ARM was then AF demagnetized to 100 mT in 11 steps. The NRM and ARM demagnetization data were analysed using the DAIE workbook (Sagnotti 2013).

We measured the anisotropy of magnetic susceptibility (AMS) of 14 cubic samples evenly distributed throughout the sampled interval, with the aim of reconstructing the magnetic fabric of the sediments. The AMS tensor both at the specimen and the site level was computed following Jelínek's statistics (Jelínek 1977, 1978) and using the software Anisoft (http://www.agico.com/software/winsoft/anisoft/).

Characterization of the magnetic mineralogy of the samples was obtained by measuring hysteresis properties (including first-order reversal curves; FORCs) from powders collected at the base or top of 15 discrete specimens across the M-B interval, including the cryptotephra SUL2-18. The hysteresis properties were measured on a MicroMag vibrating sample magnetometer (VSM model 2900, Princeton Measurements Corporation) with a maximum applied field of 1 T. From hysteresis cycles, we determined the saturation magnetization (M_S), the saturation remanent magnetization (M_{RS}) and the coercive force (B_C), following subtraction of the paramagnetic high-field susceptibility after saturation. After the hysteresis measurements, stepwise acquisition of isothermal remanent magnetization (IRM) and subsequent backfield remagnetization (both up to 1 T) was measured for each specimen to compute the remanent coercive force (B_{CR}). Finally, FORC measurements were made in steps of 2.5 mT and an averaging time of 200 or 300 ms, using a 1 T saturating field. To analyse FORC data and produce FORC diagrams, we used the FORCinel software developed by Harrison & Feinberg (2008). Finally, stepwise thermal demagnetization of

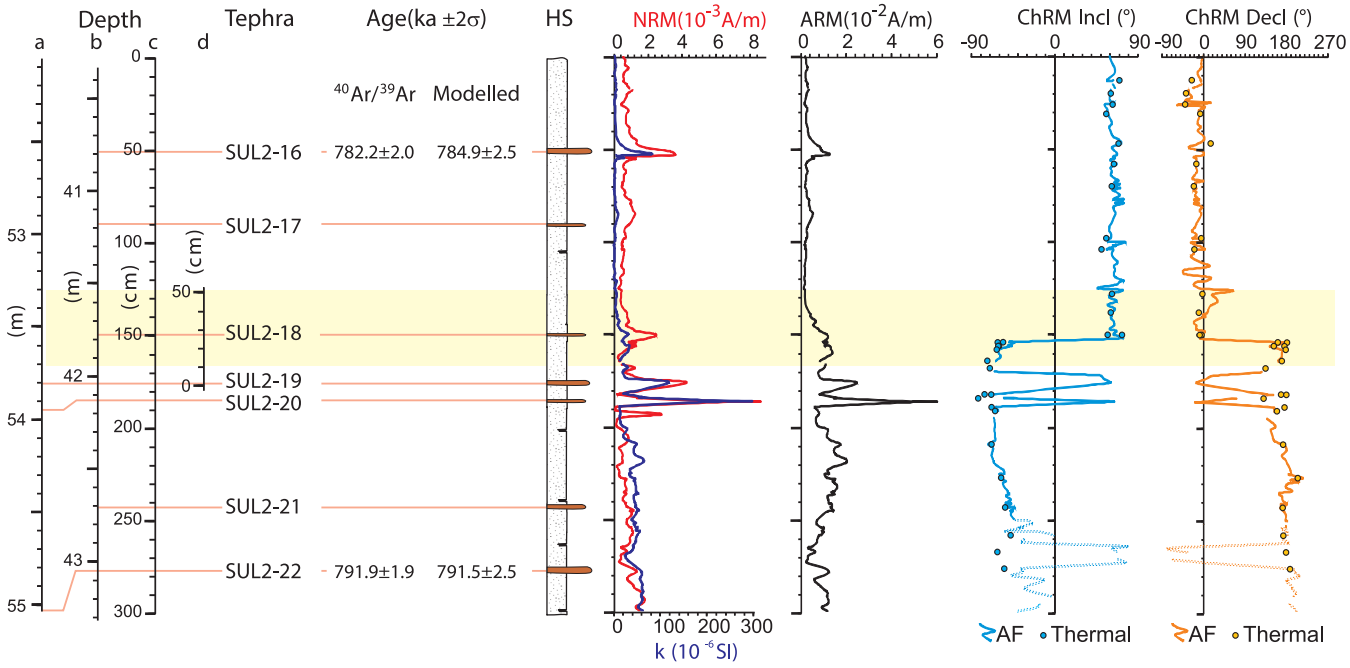

Figure 2. Stratigraphic variation of selected parameters from former palaeomagnetic investigation at the Horseshoe section (HS) (Sagnotti *et al.* 2014). The yellow bar highlights the stratigraphic interval investigated in this study. The chronological constraints—raw $^{40}Ar/^{39}Ar$ (Sagnotti *et al.* 2014; Giaccio *et al.* 2015) and the Bayesian modeled (Giaccio *et al.* 2015) ages for the tephras SUL2-16 and SUL2-22—and the different depth scales employed in previous and this study (a) Sulmona core SC1 depth, Giaccio *et al.* 2013; (b) SUL6 composite depth; Giaccio *et al.* 2015; (c) HS depth; Sagnotti *et al.* 2014; (d) HS depth; this study, are also shown.

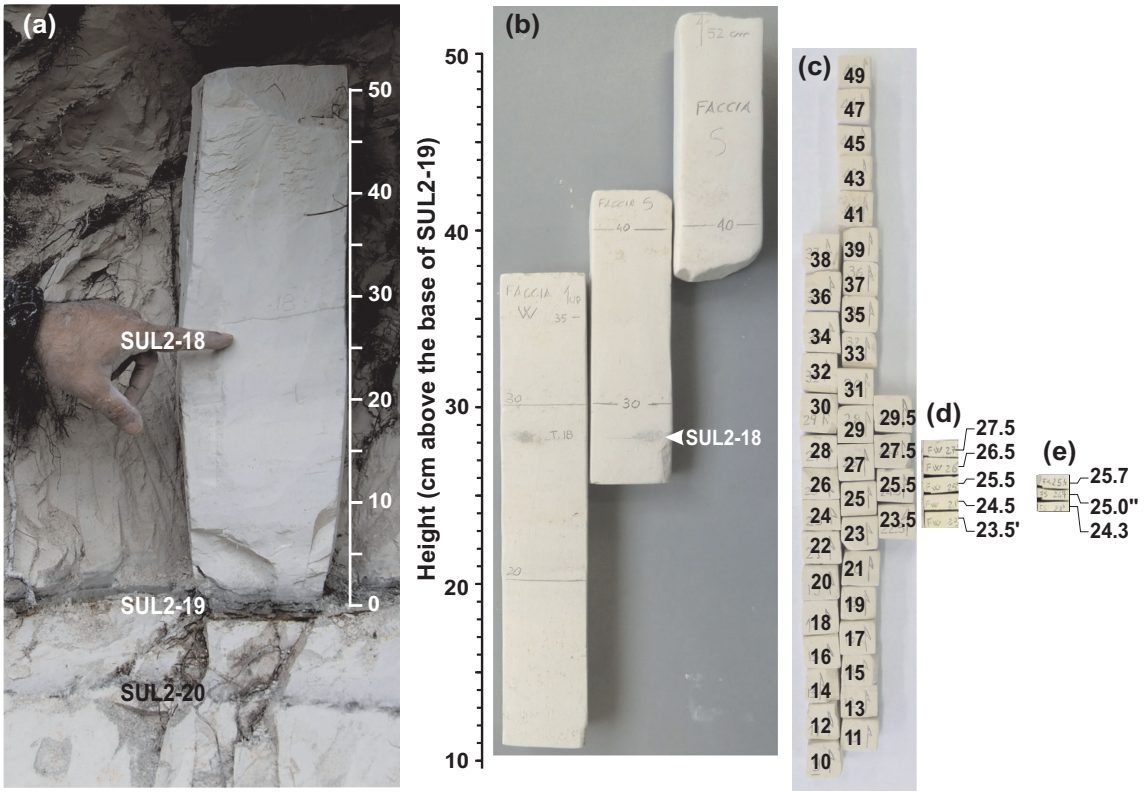

Figure 3. Sampling of the Horseshoe section. The sampled interval was isolated as a single coherent block (a). The block was cut in the laboratory in three partially overlapping columns that (b) were cut in regular columns (2 cm width) from which overlapping cubes (2 cm on a side) separated vertically by 1 cm and 0.7 cm (c) and thinner parallelepipeds of (d) ~1 and (e) 0.7 cm thick were obtained. Numbers indicate the stratigraphic height (cm) of the sample midpoint relative to the base of tephra SUL2-19. The position of tephra SUL2-18, which is visible as a millimetric and discontinuous dark veil, is highlighted.

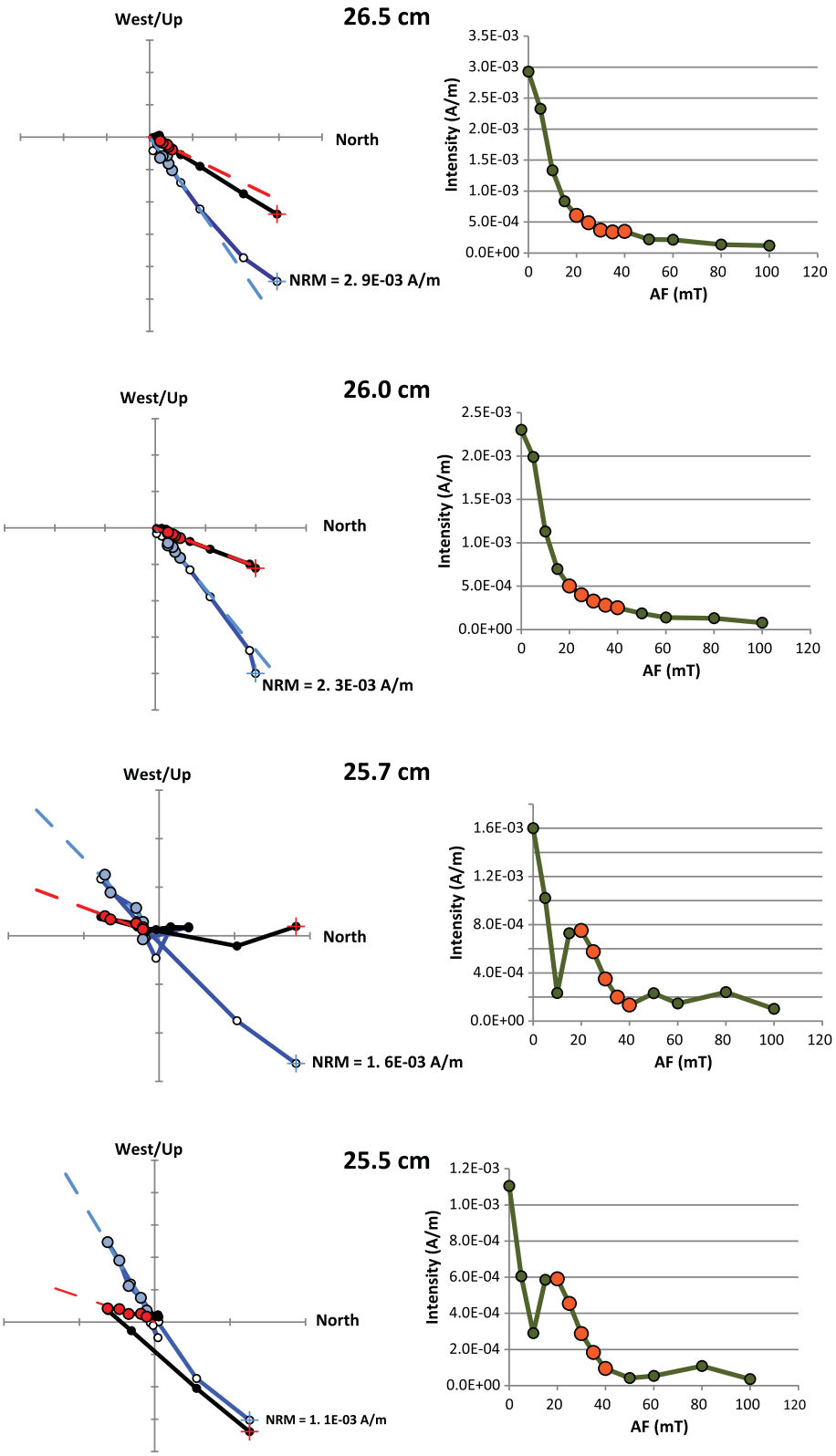

Figure 4. Representative NRM demagnetization diagrams for specimens collected immediately above (samples 26.5 and 26.0; Fig. 3) and below (samples 25.7 and 25.5 cm; Fig. 3) the M-B boundary following AF stepwise demagnetization. In the orthogonal vector diagrams (Zijderveld 1967), open and filled circles represent projections onto vertical and horizontal planes, respectively. Changes in NRM intensity at each step are shown in the plots to the right of the vector diagrams. The data selected for ChRM determination are pointed out as coloured circles (red for declination, light blue for inclination in the vector diagrams and orange in the intensity diagrams). The demagnetization data have been analysed using the DAIE workbook (Sagnotti 2013).

a composite IRM for 8 specimens was produced by the sequential application of 1, 0.5 and 0.12 T pulse fields along the three orthogonal axes (Lowrie 1990) and demagnetized in 10 steps up to 600 °C.

Finally, we characterized magnetic particles by using an FEI quanta 400 Scanning Electron Microscope, at 'La Sapienza' university of Rome, equipped with backscattered electron detector and Energy Dispersion System (EDS) microanalysis. Samples were first

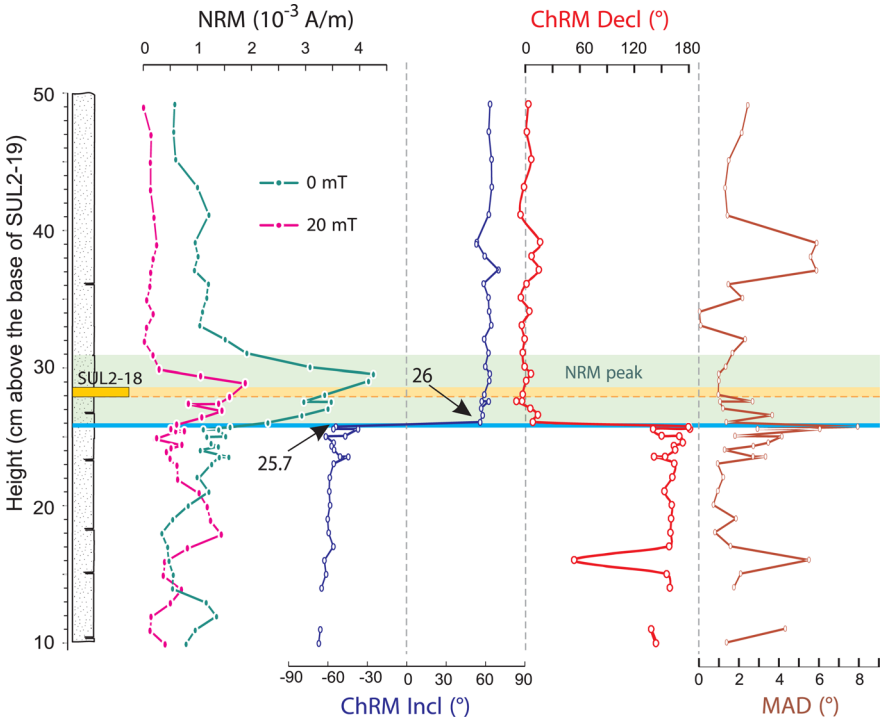

Figure 5. Stratigraphic variation of NRM intensity, ChRM inclination (Incl), ChRM declination (Decl) and associated maximum angular deviation (MAD). The blue, yellow and green horizontal bars highlight the stratigraphic intervals of the M-B polarity transition, the SUL2-18 tephra and NRM peak, respectively. The position of the uppermost sample with reverse polarity (25.7) and the lowermost sample with normal polarity (26) is also identified.

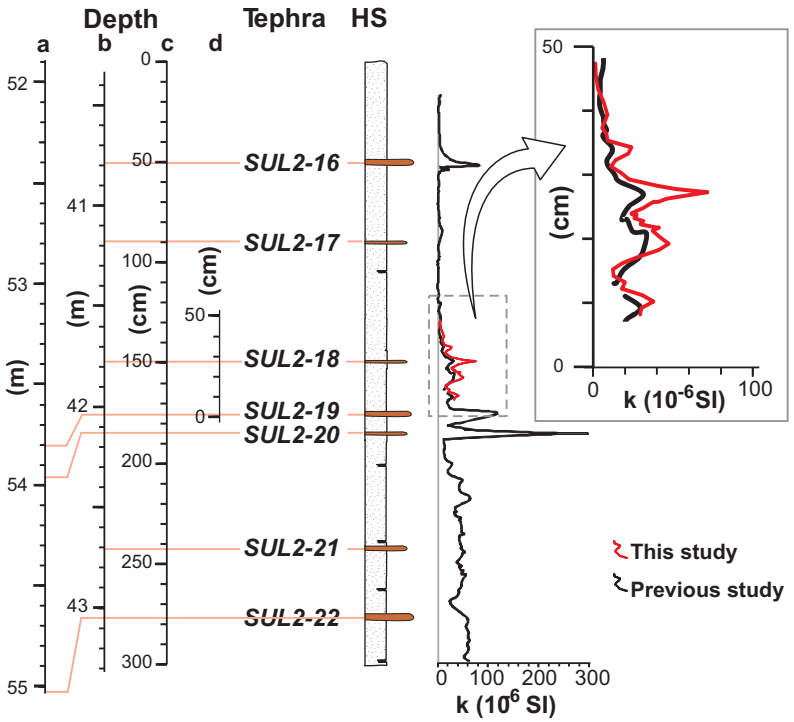

Figure 6. Magnetic susceptibility profiles allows a precise correlation of the stratigraphic interval sampled in this study (red line) with the longer stratigraphic section analysed by Sagnotti *et al.* (2014; black line). For comparison, the different depth scales employed in previous and this study [(a) core SC1 depth, Giaccio *et al.* 2013; (b) SUL6 composite depth; Giaccio *et al.* 2015; (c) HS depth; Sagnotti *et al.* 2014; (d) HS depth; this study], are also shown.

diluted in distilled water and sieved to obtained separates enriched in the heavy mineral fraction. Separates were then carbon-coated to allow EDS identification of metals and were observed using both secondary (SE) and backscattered (BSE) electrons.

RESULTS

Palaeomagnetism

As in the previous palaeomagnetic analysis of the HS section (Sagnotti *et al.* 2014) the NRM demagnetization data retrieve a well-defined characteristic remanent magnetization (ChRM), whose orientation was computed by principal component analysis (Kirschvink 1980) using at least four consecutive AF steps between 10 and 60 mT (Fig. 4). The resulting maximum angular deviation (MAD) of each ChRM determination does not exceed 8° for any of the specimens (Fig. 5) and is less than 5° for most of them. All of the samples below specimen 25.7—which is a ∼0.7-cm-thick parallelepiped whose base is 25.4 cm above the base of tephra SUL2-19 (Fig. 3e) are of reverse polarity; all of the samples above specimen 26—which is a standard 2-cm-wide cube cut with its base at 25 cm (Fig. 3c)—are of normal polarity (Figs 4 and 5). The polarity transition occurs ∼2.5 cm below the cryptotephra SUL2-18, which is recognized at ∼28 cm of this study depth scale (Fig. 5) and at 41.82 m depth of the composite SUL6 unit (Fig. 2). The polarity transition also corresponds to the initial rise of a positive peak in the NRM intensity, which reaches its maximum value at 29.5 cm (Fig. 5). The stratigraphic position of the M-B reversal closely matches that obtained previously (Sagnotti *et al.* 2014), where the terminus of the M-B reversal occurs at about 2–3 cm below cryptotephra SUL2-18, between two adjacent samples at 152 and 154 cm of the local stratigraphic framework (depth scale c in Fig. 2).

Rock magnetism

The magnetic susceptibility profile allows a high-resolution correlation of the sequence sampled in this study with that sampled by Sagnotti *et al.* (2014; Fig. 6). With the exception of tephra SUL2-18 and the sediments immediately above it, the hysteresis data indicate a mineralogical uniformity of all the samples. They show narrow hysteresis loops, steep IRM acquisition curves at fields < 0.1 T, IRM saturation at ∼0.2 T, and are characterized by a coercivity distribution with almost closed and narrow FORC contours peaked around B_C values of 15–25 mT (Fig. 7). Conversely, the sample collected from tephra SUL2-18 shows a broader hysteresis loop, its IRM is far from saturation at 0.2 T, and its FORC coercivity distribution is characterized by wider contours and a long tail along the B_C axis, extending beyond 100 mT (Fig. 7).

The plot of the hysteresis ratios M_{RS}/M_S versus B_{CR}/B_C (Day *et al.* 1977) indicates that the lacustrine sediments not including SUL2-18 fall within the theoretical mixing lines for pseudo-single domain (PSD) magnetite grains or for variable mixtures of single

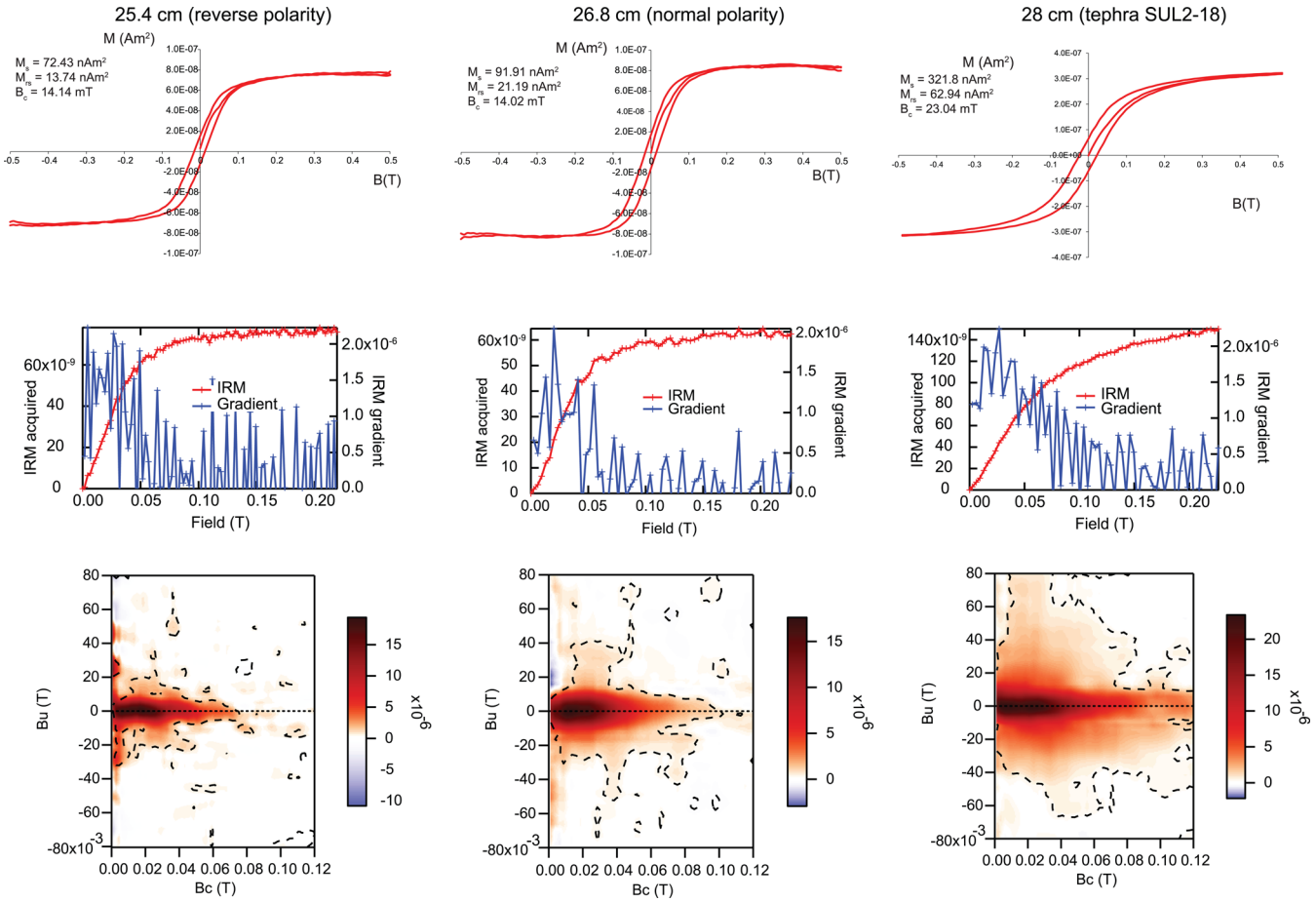

Figure 7. Hysteresis loops (upper plots), isothermal remanence (IRM) acquisition curves (middle plots) and FORC diagrams (lower plots) for representative samples collected at 25.4 cm (reverse polarity), 26.8 cm (normal polarity) and 28 cm (tephra SUL2-18). The dashed lines in FORC diagrams indicate where signal to noise ratio is greater than a threshold of 3.

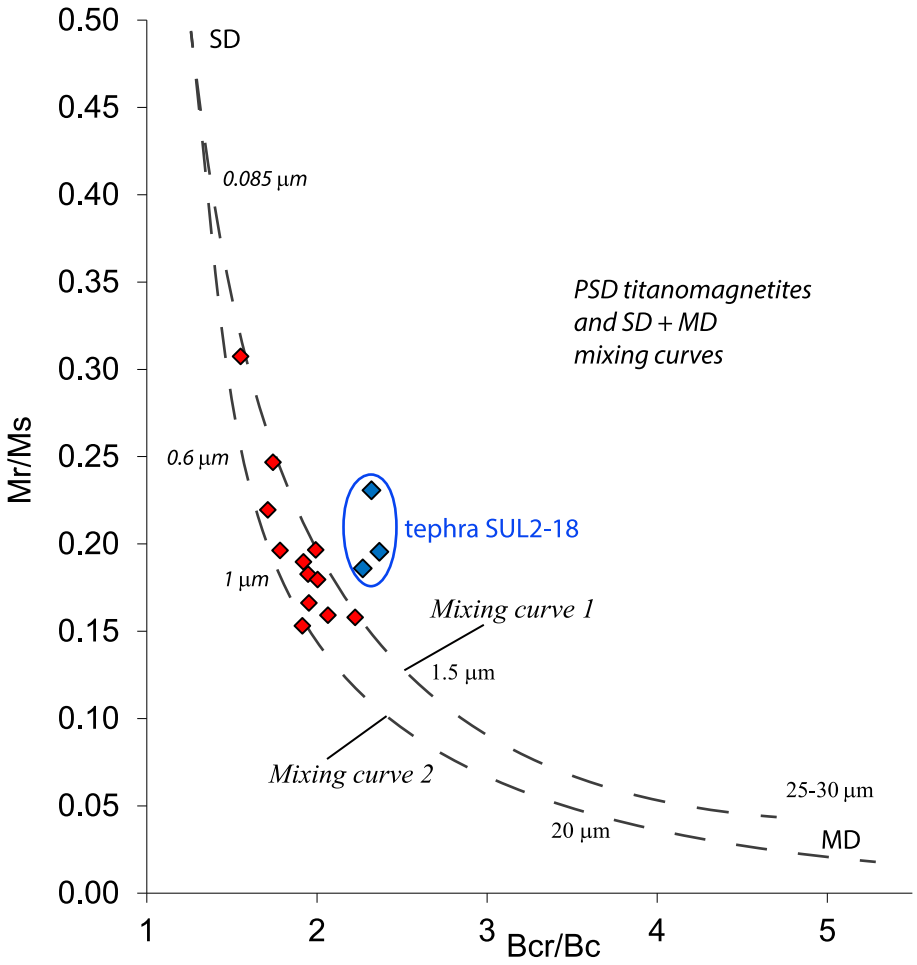

Figure 8. Plot of hysteresis ratios (M_{rs}/M_s versus B_{cr}/B_c) for the various measured specimens (after Day *et al.* 1977). The data referring to the all the sediments not affected by tephra SUL2-18 (red diamonds) fall within the theoretical curves calculated for mixtures of single domain (SD) and multidomain (MD) titanomagnetite grains, indicated by the dashed lines (after Dunlop 2002). The data from the samples affected by tephra SUL2-18 (blue diamonds; collected at 27.8, 28 and 29 cm) are distinct and plot above and to the right of the SD + MD titanomagnetite mixing curves.

domain (SD) and multidomain (MD) magnetite particles (Dunlop 2002; Fig. 8). Conversely, the data from powders collected from tephra SUL2-18 and from the sediments immediately above it fall in a distinct region of the Day plot, pointing to a different population of magnetic grains (Fig. 8).

The thermal demagnetization of the composite IRM shows that: (i) the IRM is mostly held by the low-coercivity axis (*X*, applied field 0.12 T) and the high-coercivity component (*Z*, applied field 1 T) is almost zero for all samples, (ii) the IRM is mostly removed below 450 °C (as it is for the NRM; Sagnotti *et al.* 2014) and (iii) the maximum unblocking temperature is about 550 °C (Fig. 9). In agreement with the hysteresis data, these results indicate that the main carrier of the remanence in all of the lacustrine samples is Ti-poor titanomagnetite in a PSD magnetic state.

The demagnetization for the cubic sample spanning the 27–29 cm stratigraphic interval is slightly different with respect to all the other samples, as seen also in the hysteresis data. We note a distinctly higher contribution of the intermediate-coercivity fraction (*Y*, applied field 0.5 T), suggesting that tephra SUL2-18 is characterized by a population of magnetic particles with a wider coercivity distribution (skewed toward higher values) with respect to that found in the other lacustrine sediment samples, as indicated by the hysteresis properties (Fig. 7).

SEM observations show that the sediment is composed of biogenic carbonates with abundant diatom frustules (Fig. 10a). Magnetic minerals were identified as micrometre-sized magnetite grains forming framboidal (sample 22 cm) or irregular (sample 26 cm) aggregates in the lacustrine sediments (Figs 10b and c). Conversely, in the SUL2-18 tephra layer (28 cm) there are abundant volcanic components and magnetic minerals have been identified in smaller aggregates of magnetite crystals (Fig. 10d).The AMS measurements indicate that the degree of anisotropy for most of the samples is very low ($P < 1.01$). Nevertheless, the data indicate that the AMS tensor is relatively well defined at the site level and is characterized by an almost vertical minimum susceptibility axis and maximum and intermediate susceptibility axis widely scattered in the bedding plane (Fig. 11).

A synopsis of the stratigraphic distribution of the main palaeomagnetic and rock magnetic parameters is provided in Fig. 12.

DISCUSSION

The AMS fabric of the sediments (Fig. 11) is consistent with a sedimentary-compactional fabric and indicates that the sequence was not affected by significant post-depositional deformation. The consistency of the various data profiles collected from different sections of the same stratigraphic interval also indicates that the

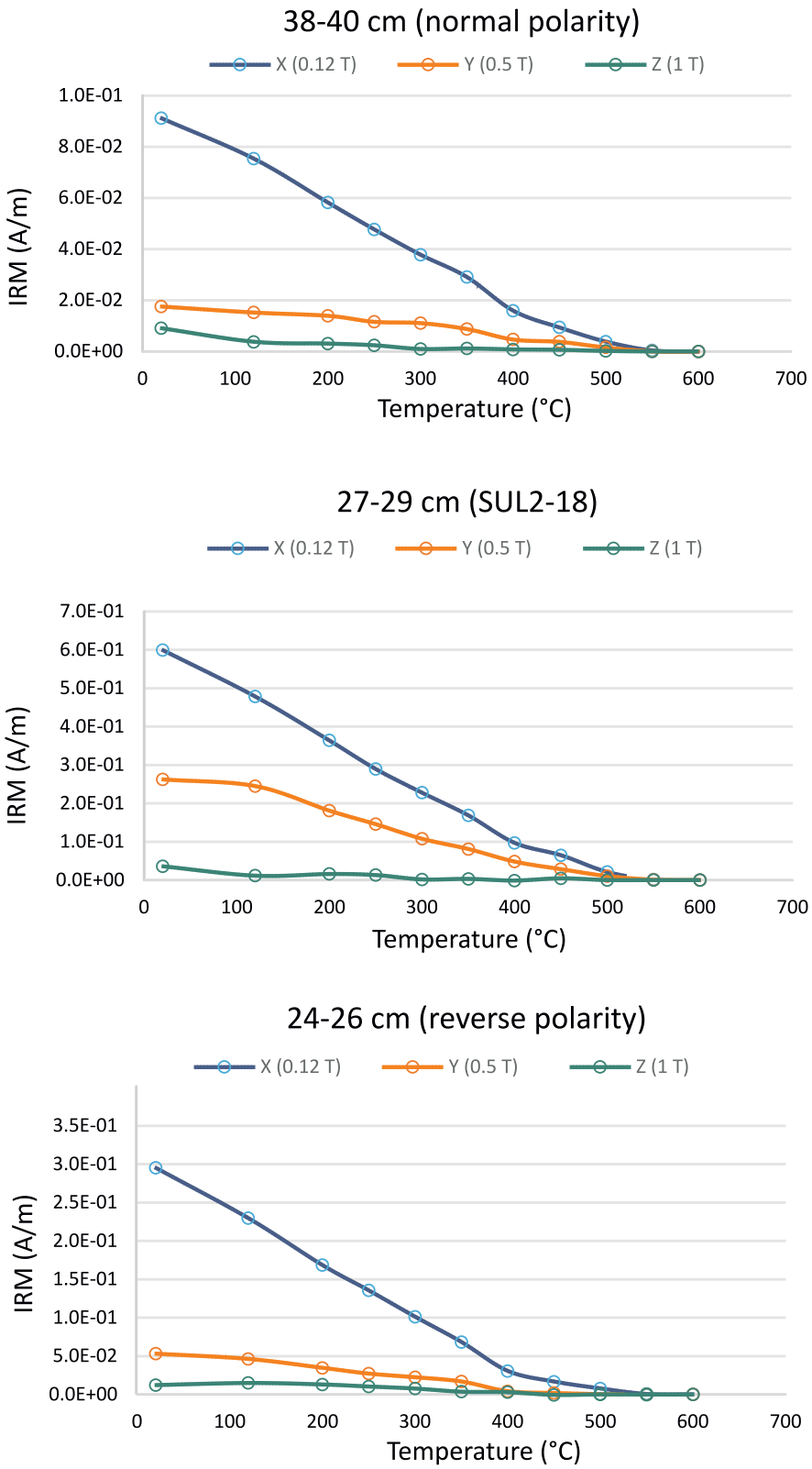

Figure 9. Thermal demagnetization of a composite IRM (Lowrie 1990).

original stratigraphic framework is well preserved and highlights a remarkable lateral continuity. This is also confirmed by the sedimentologic features of the tephra layers occurring in the SUL6 unit. Throughout the basin they systematically show a sharp basal contact, a uniform thickness and a consistent internal structure (e.g. vertical grading and lithological and geochemical zonation); all of these features indicate a pure fallout origin and a rather negligible or even no post-depositional reworking.

This study demonstrates that the final VGP transit associated to the M-B geomagnetic field reversal is recorded in different outcrops

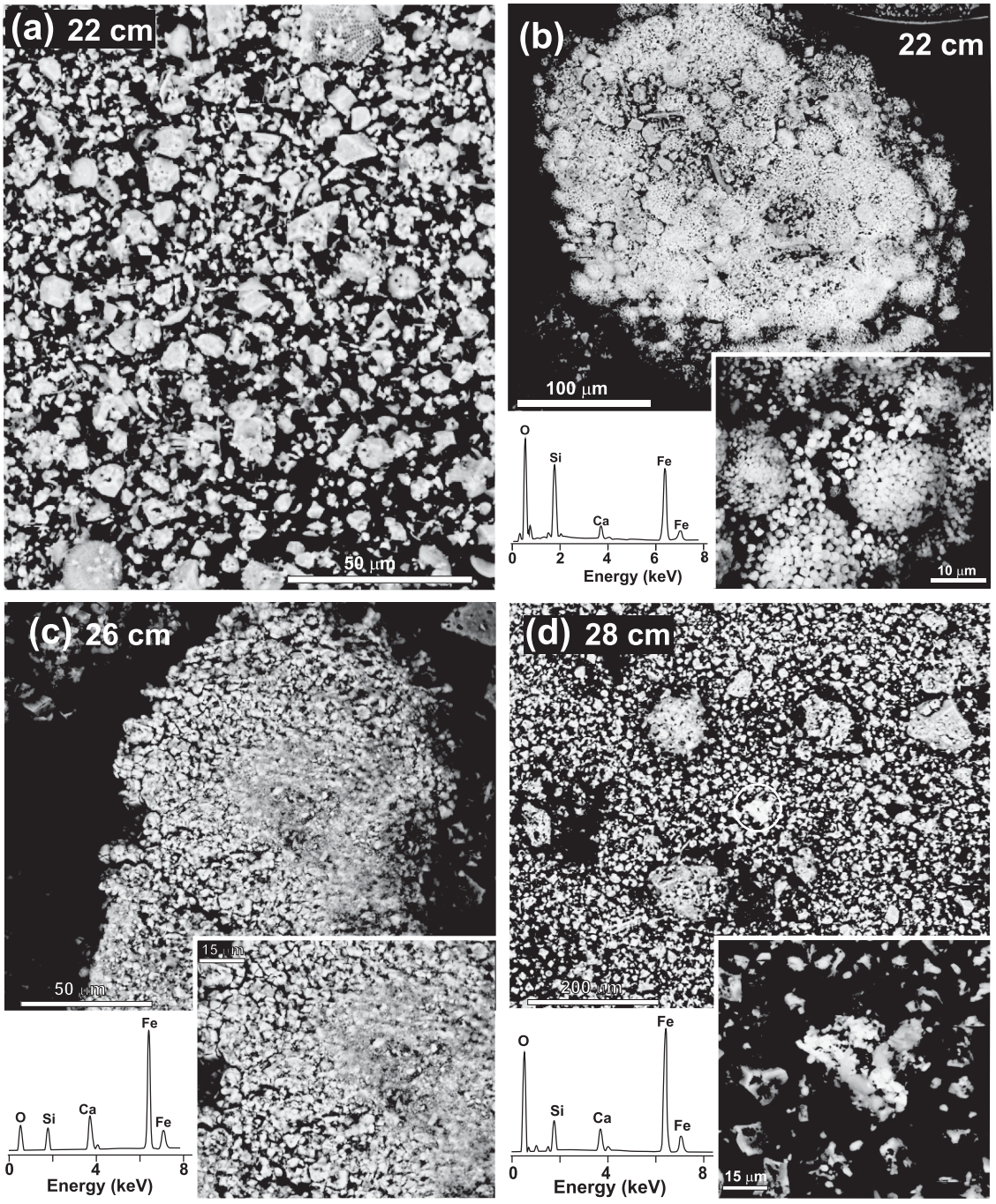

Figure 10. BSE images of samples from selected depths and corresponding EDS spectra (labels mark the Kα peaks of major elements). (a) Overview of the bulk sediment character at 22 cm depth, (b) aggregate of framboidal magnetite micrometre-sized crystals and diatom tests from separate at 22 cm depth, (c) irregular aggregate of magnetite particles from separate at 26 cm depth and (d) overview of the sediment character at 28 cm depth (SUL2-18 tephra layer), with magnification of an irregular aggregate of magnetite particles (circled in the large-scale photograph).

of the HS section as a sharp event occurring 2–3 cm below cryptotephra SUL2-18 (about 28 cm above SUL2-19) with no record of intermediate VGP positions. This stratigraphic position is also in excellent agreement with the lower resolution data from the SC1 core (Giaccio *et al.* 2013; contra Suganuma *et al.* 2015), which was drilled at a distance of ∼500 m NNW from HS site (Fig. 1a), where the MBB was constrained in the interval between 51.86 (normal polarity) and 53.63 m (reverse polarity) (see Fig. 2 for the comparison of the different depth scales). Due to its low resolution, the earliest palaeomagnetic study of the SC1 core (Giaccio *et al.* 2013), was not suitable to precisely constrain the stratigraphic position of the M-B directional change. However, new analyses carried out at 1-cm spacing on u-channel samples collected from the SC1 core reveal that the rock magnetic and palaeomagnetic record of the SC1 core can be closely matched to those obtained in the HS subsections and that the M-B polarity flip occurs at the same stratigraphic position (Fig. 13).

The sedimentation rate in the HS section was computed as 0.35 mm yr^{-1} by the Bayesian model of the precisely determined $^{40}Ar/^{39}Ar$ ages of several tephra layers intercalated in the calcareous

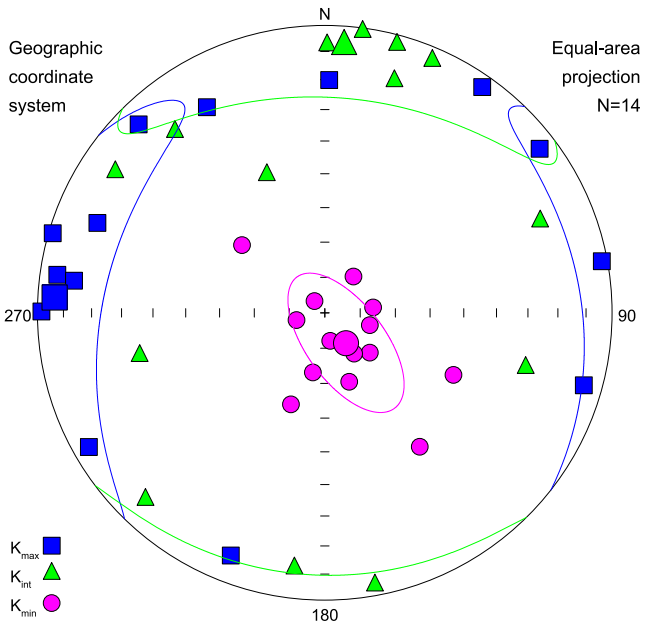

Figure 11. Magnetic anisotropy (AMS) data; equal-area Schmidt projection, lower hemisphere. The ellipses indicate the 95 per cent region around the principal susceptibility axes.

lacustrine sequence (Giaccio *et al.* 2015). This estimation is remarkably consistent with the temporal progression and the astronomical pacing of the MIS 19c interglacial as documented in worldwide reference records (Giaccio *et al.* 2015). Anyway, in order to obtain an estimation more strictly related to the short stratigraphic interval investigated and its inherent chronological uncertainty, we here use a simple linear interpolation of the two ages of the tephra SUL2-16 and SUL2-22, with propagation of related full analytical uncertainty, which yields a mean sedimentation rate of 0.28 ± 0.12 mm yr^{-1} for the interval deposited between the two tephras encompassing the M-B reversal. In the former analysis, the M-B VGP transit was constrained between two consecutive cubic specimens that are 2 cm on a side, implying that it occurred in less than a century (Sagnotti *et al.* 2014). We now can refine this estimate and show that the M-B VGP transit is systematically recorded ∼2–3 cm below the tephra SUL2-18 as an abrupt change between two consecutive specimens in all the five overlapping columns of samples obtained from the single block analysed in this study (Figs 3d and e). Specifically, the terminus of the M-B transition can be precisely constrained between the uppermost reverse specimen 25.7, which is the 0.7-cm-thick parallelepiped sample spanning the 25.3–26.0 cm stratigraphic interval and the lowermost normal specimen 26, which is a 8 cc cube spanning the 25–27 cm stratigraphic interval, above the base of tephra SUL2-19 (Figs 3 and 12). This finding confirms that the record of the M-B VGP transit is extremely sharp and occurs within the very thin stratigraphic interval matching the difference between the stratigraphic heights of the narrowly overlapped 25.7 and 26 specimens; that is, ∼0.3 cm, which corresponds to ∼8 yr according to the Bayesian age model of Giaccio *et al.* (2015) or to 13 ± 6 yr, according to the linear interpolation and related full uncertainty. Thus, the new data refine the former constraints on the duration of the interval recording the end of the M-B polarity transit in the Sulmona Basin by an order of magnitude.

The VGP path spanning the M-B polarity transit obtained by the new palaeomagnetic data is remarkably similar to the one presented in Sagnotti *et al.* (2014), with a sudden jump of the VGP from the southern polar region to the northern one without intermediate positions recorded (Fig. 14a). We point out that this new study at higher resolution also confirms the presence of a limited but clear VGP loop toward the Kerguelen Island before the final VGP transit and identifies a possible earlier larger geomagnetic excursion toward the

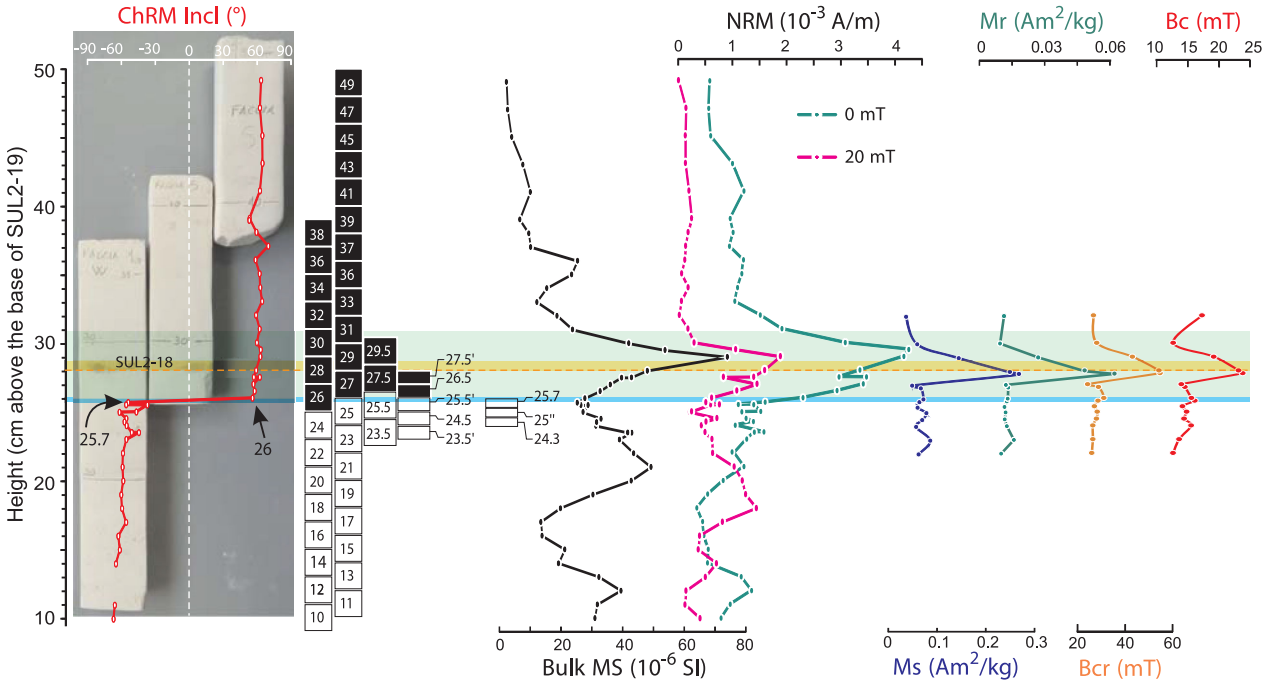

Figure 12. Overlapping columns, with superimposed ChRM inclination (Incl) plot, and discrete specimens cut from the collected block and stratigraphic variation of the main palaeomagnetic and rock magnetic properties. Each specimen is indicated by black or white boxes according to its magnetic polarity (white reversed and black normal). The blue, yellow and green horizontal bars highlight the stratigraphic position of the M-B polarity transition, the SUL2-18 tephra and NRM peak, respectively.

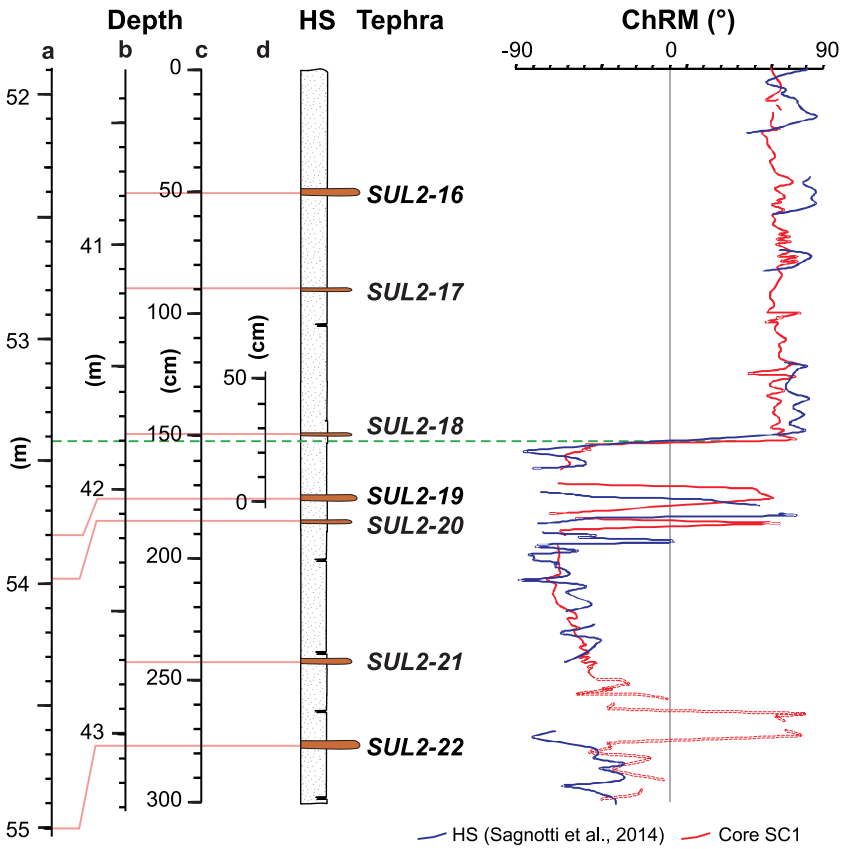

Figure 13. ChRM inclination records of the Horseshoe section (Sagnotti *et al.* 2014) and the SC1 core. Data from the Horseshoe section were obtained on discrete samples (standard palaeomagnetic cubes of 2 cm side), whereas data from the SC1 core were retrieved at 1 cm spacing from u-channel samples collected from the available slices of the SC1 core. The ChRM inclination records indicate that the M-B polarity flip occurs at the same stratigraphic position in the two stratigraphic sections. The different depth scales employed in previous and this study are also shown [(a) Sulmona core SC1 depth, Giaccio *et al.* 2013; (b) SUL6 composite depth; Giaccio *et al.* 2015; (c) HS depth; Sagnotti *et al.* 2014; (d) HS depth; this study].

Solomon Islands, though it is indicated by a single specimen only. Furthermore, the adopted sampling strategy ensures that the data are not affected by smoothing effects due to continuous measurements with u-channels (e.g. Roberts 2006). Indeed, although the M-B transit identified in SC1 core occurs at the same stratigraphic position of the HS subsections, the associated VGPs are spread along an apparent path of intermediate positions spanning about 10–15 cm (Figs 13 and 14b). This apparent VGP path is clearly an artefact due to the smoothing associated to the SQUIDs response function, which reduces the resolution achievable with u-channel measurements.

The rock magnetic data point out that the magnetic mineralogy of the lacustrine samples just above and below the M-B VGP transit is remarkably homogeneous. SEM observations indicate that magnetic minerals consist of micrometre-sized (PSD) magnetite crystals occurring in aggregates of framboidal and irregular shape (Fig. 10). The occurrence of framboidal magnetite has been recently reported in lacustrine present-day sediments as a biogenic product related to dissimilatory iron reduction (Percak-Dennett *et al.* 2013). Taking into account that in this interval the concentration of biogenic carbonate reaches 90 wt per cent of the overall sediment composition (Giaccio *et al.* 2015), and that therefore the detrital fraction in the analysed interval is virtually negligible, we conclude that magnetite must be dominantly of biogenic origin in the Sulmona lacustrine sediments. We knew, however, that large and sharp peaks in concentration dependent rock magnetic parameters (*k*, NRM and ARM) are associated with thin (4–6 cm) intervals of sediments on top of tephra layers SUL2-19 and SUL2-20 (Sagnotti *et al.* 2014). The magnetic mineralogy in these intervals is different from that of the rest of the section and consists of a population of magnetic grains characterized by a coercivity distribution skewed toward distinctly higher values. The peaks in rock magnetic properties on top of tephras SUL2-19 and SUL2-20, which were deposited during the Matuyama Chron, correspond to samples of palaeomagnetic normal polarity. We therefore inferred that these thin intervals were remagnetized during the Brunhes Normal Chron, either by post-deposition growth of magnetite or by a delayed remanence lock-in. Both processes may have been favoured by the fabric of the sediment intermixed with volcanic ash. Alternatively, it is even possible, though unlikely, that samples on top of tephras SUL2-19 and SUL2-20 just fortuitously recorded actual geomagnetic precursory flickers, such as those seen immediately prior the M-B transition in cores from ODP Site 983 and Site 984 in the North Atlantic (Channell *et al.* 2010). In any case, we here show that, even if cryptotephra SUL2-18 is by far fainter than tephras SUL2-19 and SUL2-20, it is similarly associated with a distinct peak in the NRM and *k* profiles (Fig. 12) and also shares the same magnetic mineralogy of the intervals on top of SUL2-19 and SUL2-20. It is therefore likely that also cryptotephra SUL2-18 is associated with a thin remagnetized layer of 1–2 cm just above its top. The hysteresis parameters and their stratigraphic trends (Figs 8 and 12) indicate that the peculiar distinct magnetic mineralogy spans only a couple of cm above SUL2-18.

Even if the magnetic mineralogy of the samples above and below the M-B VGP transit looks exactly the same, the close proximity

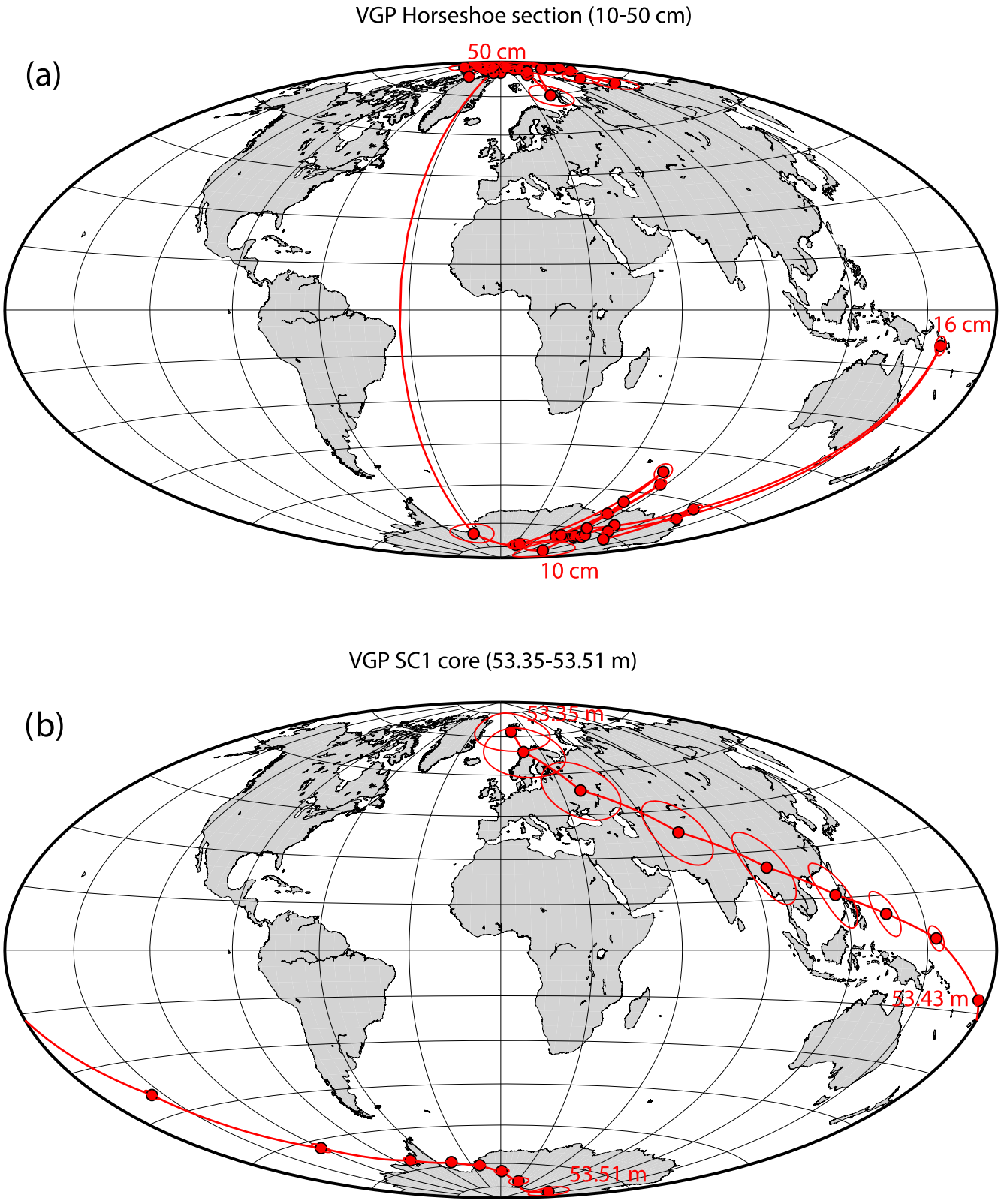

Figure 14. Schematic representation of the VGP path reconstructed from the ChRM directions determined on discrete samples from this study. Ellipses around VGP individual positions represent areas of 95 per cent confidence, that were computed from MAD values about individual ChRM directions. The upper plot (a) refers to VGP reconstructed from ChRM directions determined on discrete samples from this study (the stratigraphic interval in parentheses is referred to this study depth scale; 'd' in Fig. 2). The VGP position near the Solomon Islands (NE of Australia) is related to the large declination swing recorded by the sample centred at a stratigraphic height of 16 cm (Fig. 5). The lower plot (b) refers to VGP reconstructed from ChRM directions determined on u-channel samples collected from core SC1 (authors' unpublished data; declination is arbitrary, the stratigraphic interval in parentheses refers to the SC1 depth scale, indicated as scale 'b' in Fig. 2).

of the cryptotephra SUL2-18, whose presence affects the sediment magnetic properties, suggests caution in the palaeomagnetic interpretation. In fact, the NRM intensity stratigraphic profile shows a major peak that starts 2 cm below and ends 4 cm above SUL2-18. The early NRM rise coincides with the M-B polarity flip (Fig. 5). The entire set of rock magnetic data indicates that the disturbance induced by SUL2-18 of the rock magnetic properties of the sediments spans at most ∼3 cm on both the upper and lower sides of the cryptotephra.

The new data allow us to conclude that there are two ways to interpret the palaeomagnetic record of the M-B reversal from the HS section. The first possibility is that the presence of tephra SUL2-18 induced the remagnetization of an interval of about 6 cm around it (i.e. the whole thickness of the NRM peak) and the detailed record of the M-B VGP transit is lost because it was overprinted in that interval. In this hypothesis, the maximum duration for the M-B transit is ∼260 ± 110 yr according to the local sedimentation rate. The second possibility is that the palaeomagnetic record below SUL2-18 is fully reliable and the M-B VGP transit occurred about 2 cm below SUL2-18 (i.e. less than a century before) during an interval of less than 0.3 cm and therefore lasted less than 13 ± 6 yr. A very rapid polarity flip is consistent with the model of geomagnetic field variation proposed by Brown *et al.* (2007), who suggested that the directional reversal may take place in less than 10 yr at a regional scale and that individual reversal records have the potential to be different at different locations assuming that reversals are related to behaviour of the dipole field separate from that of the non-dipole field (and thus secular variation). Brown *et al.* (2007) also implies that a rapid reversal at one location may be compatible with a much longer duration reversal elsewhere. It is therefore difficult to extrapolate at a global scale features observed from a single reversal record, as well as interferences about its duration. We note anyway that a fast (i.e. <1 ka) polarity flip is indicated by the best palaeomagnetic transition records available from globally distributed lava flows (Valet *et al.* 2012) and a duration at a decadal scale of the M-B flip was also inferred from the palaeomagnetic analysis of marine sediments in Japan (Okada & Niitsuma 1989). Also, the final directional change at the terminus of the M-B transition is recorded in just a few centimetre in the u-channel palaeomagnetic record of several north Atlantic cores (Channell *et al.* 2010), which is a feature compatible with a very rapid polarity flip.

CONCLUSIONS

The HS section in the Sulmona Basin shows many of the properties required to preserve an excellent record of geomagnetic field changes during the M-B reversal. In particular, the section ensures: (i) an evident stratigraphic integrity and continuity, (ii) good palaeomagnetic properties with easily interpretable demagnetization diagrams, (iii) a remarkable homogeneity of the magnetic mineralogy, with magnetite as the main remanence carrier (and identifiable subtle changes linked to tephra layers and potential associated remagnetization) and (iv) a highly precise chronological framework. All these features make the HS section an ideal sedimentary succession for preserving a continuous record of the M-B reversal and for precisely assessing the tempo of the magnetic directional change. On the other hand, the Sulmona lacustrine record is, of course, not free from smoothing effects on the palaeomagnetic record due the natural NRM acquisition processes during dewatering and compaction of the sediments and from possible effects associated to an unknown, and currently indeterminable, lock-in function that may have shifted downward the stratigraphic position of the palaeomagnetic record. In any case, this study confirms that the record of the M-B polarity transit in the Sulmona Basin is extremely sharp. The very sharp character of the polarity transition record cannot be accounted for by any sedimentary smoothing effect or lock-in function. Furthermore, the observation that M-B polarity transit occurs at the same stratigraphic position of both outcropping (previous and present HS sites) and cored (SC1) sections, provides robust evidence for a primary remanent magnetization, since it is unlikely that remagnetization occurred at precisely the same spot in distinct sections. It is also clear that the sediments immediately above and below the polarity transit share exactly the same magnetic mineralogy. We further recognize that the occurrence of tephra layers correspond to subtle changes in the magnetic mineralogy, with the sediments deposited on top of some of these tephra layers containing a population of magnetite grains with a coercivity distribution toward distinctly higher values than the rest of the lacustrine sediments. We recognize that thin intervals of sediments on top of some tephra layers SUL2-19 and SUL2-20 were potentially remagnetized after the M-B geomagnetic reversal (Fig. 2). Therefore, the occurrence of tephra layers may compromise the fidelity of the palaeomagnetic record, though they provided essential age constraints that still allow establishing a robust chronology for the sedimentary succession. We conclude that while adopting the more cautious interpretation, though not necessarily more convincing, that tephra SUL2-18 corrupted the recording of the actual geomagnetic field behaviour; this disturbance may have overprinted the record for three–four centuries at most. A very fast rate of the VGP transit (e.g. a polarity flip occurring at a decadal timescale), as a genuine geomagnetic feature developed during the last geomagnetic polarity reversal, remains a hypothesis that is well supported by the current data.

ACKNOWLEDGEMENTS

We are deeply grateful to Michael E. (Ted) Evans for his interesting remarks on our formerly published manuscript on the Horseshoe section. His insightful comments stimulated the research presented in this paper. We also acknowledge Mark Bourne, for his help in the analysis of FORC diagrams and for his general comments to the manuscript, which allowed us to improve the originally submitted version. We thank Marco Albano for his assistance with SEM observations and EDS analyses.

REFERENCES

Biggin, A.J., Steinberger, B., Aubert, J., Suttie, N., Holme, R., Torsvik, T.H. & Van Hinsbergen, D.J.J., 2012. Possible links between long-term geomagnetic variations and whole-mantle convection processes, *Nature Geosci.,* **5**(8), 526–533.

Brown, M.C., Holme, R. & Bargery, A., 2007. Exploring the influence of the non-dipole field on magnetic records for field reversals and excursions, *Geophys. J. Int.,* **168**(2), 541–550.

Channell, J.E.T., Hodell, D.A., Singer, B.S. & Xuan, C., 2010. Reconciling astrochronological and $^{40}Ar/^{39}Ar$ ages for the Matuyama-Brunhes boundary and late Matuyama Chron, *Geochem. Geophys. Geosyst.,* **11,** Q0AA12, doi:10.1029/2010GC003203.

Coe, R.S. & Glen, J.M.G., 2004. The complexity of reversals, in *Timescales of the Paleomagnetic Field*, pp. 221–232, eds Channell, J.E.T., Kent, D.V., Lowrie, W. & Meert, J.G., American Geophysical Union, Washington.

Day, R., Fuller, M. & Schmidt, V.A., 1977. Hysteresis properties of titanomagnetites. Grain-size and compositional dependence, *Phys. Earth Planet. Inter.,* **13,** 260–267.

Dunlop, D.J., 2002. Theory and application of the Day plot (Mrs/Ms versus Hcr/Hc): 1. Theoretical curves and tests using titanomagnetite data, *J. geophys. Res.,* **107**(B3), 2056, doi:10.1029/2001JB000486.

Galli, P., Giaccio, B., Peronace, E. & Messina, P, 2015. Holocene paleoearthquakes and early-late pleistocene slip-rate on the Sulmona Fault (Central Apeninnes, Italy), *Bull. seism. Soc. Am.,* **105,** 1–13.

Giaccio, B. *et al.* 2012. The late MIS 5 Mediterranean tephra markers: a reappraisal from peninsular Italy terrestrial records, *Quat. Sci. Rev.,* **56,** 31–45.

Giaccio, B., Castorina, F., Nomade, S., Scardia, G., Voltaggio, M. & Sagnotti, L., 2013. Revised chronology of the Sulmona lacustrine succession, Central Italy, *J. Quaternary Sci.,* **28,** 545–551.

Giaccio, B. *et al.,* 2015. Duration and dynamics of the best orbital analogue to the present interglacial, *Geology,* **43,** 603–606.

Harrison, R.J. & Feinberg, J.M., 2008. FORCinel: an improved algorithm for calculating first-order reversal curve distributions using locally weighted regression smoothing, *Geochem. Geophys. Geosyst.,* **9,** Q05016, doi:10.1029/2008GC001987.

Hyodo, M., 1984. Possibility of reconstruction of the past geomagnetic field from homogeneous sediments, *J. Geomag. Geoelectr.,* **36,** 45–62.

Jelínek, V., 1977. The statistical theory of measuring anisotropy of magnetic susceptibility of rocks and its application, *Geofyzika, Brno,* **87**(3), 4 (Available at: http://www.agico.com/manuals/ap01.pdf).

Jelínek, V., 1978. Statistical processing of anisotropy of magnetic susceptibility measured on groups of specimens, *Stud. Geophys. Geod.,* **22,** 50–62.

Kirschvink, J.L., 1980. The least-squares line and plane and the analysis of paleomagnetic data, *Geophys. J. R. astr. Soc.,* **62,** 699–718.

Liu, Q.S., Roberts, A.P., Rohling, E.J., Zhu, R.X. & Sun, Y.B., 2008. Post-depositional remanent magnetization lock-in and the location of the Matuyama–Brunhes geomagnetic reversal boundary in marine and Chinese loess sequences, *Earth planet. Sci. Lett.,* **275,** 102–110.

Lowrie, W., 1990. Identification of ferromagnetic minerals in a rock by coercivity and unblocking temperature properties, *Geophys. Res. Lett.,* **17,** 159–162.

Mellström, A., Nilsson, A., Stanton, T., Muscheler, R., Snowball, I. & Suttie, N., 2015. Post-depositional remanent magnetization lock-in depth in precisely dated varved sediments assessed by archaeomagnetic field models, *Earth planet. Sci. Lett.,* **410,** 186–196.

Okada, M. & Niitsuma, N., 1989. Detailed paleomagnetic records during the Brunhes-Matuyama geomagnetic reversal, and a direct determination of depth lag for magnetization in marine sediments, *Phys. Earth Planet. Int.,* **56**(1) 133–150.

Percak-Dennett, E.M., Loizeau, J.L., Beard, B.L., Johnson, C.M. & Roden, E.E., 2013. Iron isotope geochemistry of biogenic magnetite-bearing sediments from the Bay of Vidy, Lake Geneva, *Chem. Geol.,* **360,** 32–40.

Regattieri, E., Giaccio, B., Zanchetta, G., Drysdale, R.S., Galli, P., Peronace, E., Nomade, S. & Wulf, S., 2015. Hydrological variability over Apennine during the Early Last Glacial precession minimum, as revealed by a stable isotope record from Sulmona basin, Central Italy, *J. Quaternary Sci.,* **30,** 19–31.

Roberts, A.P., 2006. High-resolution magnetic analysis of sediment cores: strengths, limitations and strategies for maximizing the value of long-core magnetic data, *Phys. Earth planet. Inter.*, **156,** 162–178.

Roberts, A.P. & Winklhofer, M., 2004. Why are geomagnetic excursions not always recorded in sediments? Constraints from post-depositional remanent magnetization lock-in modelling, *Earth planet. Sci. Lett.,* **227,** 345–359.

Sagnotti, L., 2013. Demagnetization Analysis in Excel (DAIE)—an open source workbook in Excel for viewing and analyzing demagnetization data from paleomagnetic discrete samples and u-channels, *Ann. Geophys.,* **56,** D0114, doi:10.4401/ag-6282.

Sagnotti, L., Budillon, F., Dinarés-Turell, J., Iorio, M. & Macrì, P., 2005. Evidence for a variable paleomagnetic lock-in depth in the Holocene sequence from the Salerno Gulf (Italy): implications for "high-resolution" paleomagnetic dating, *Geochem. Geophys. Geosyst.,* **6**(11), doi:10.1029/2005GC001043.

Sagnotti, L., Scardia, G., Giaccio, B., Liddicoat, J.C., Nomade, S., Renne, P.R. & Sprain, C.J., 2014. Extremely rapid directional change during Matuyama-Brunhes geomagnetic polarity reversal, *Geophys. J. Int.,* **199** (2), 1110–1124.

Suganuma, Y., Okuno, J., Heslop, D., Roberts, A.P., Yamazaki, T. & Yokoyama, Y., 2011. Post-depositional remanent magnetization lock-in for marine sediments de-duced from 10Be and paleomagnetic records through the Matuyama–Brunhes boundary, *Earth planet. Sci. Lett.,* **311,** 39–52.

Suganuma, Y. *et al.,* 2015. Age of Matuyama-Brunhes boundary constrained by U-Pb zircon dating of a widespread tephra, *Geology,* **43**(6), 491–494.

Valet, J.-P., Fournier, A., Courtillot, V. & Herrero-Bervera, E., 2012. Dynamical similarity of geomagnetic field reversals, *Nature,* **490,** 89–94.

Verosub, K.L. 1977. Depositional and postdepositional processes in the magnetization of sediments, *Rev. Geophys.,* **15**(2), 129–143.

Zijderveld, J.D.A., 1967. A.C. demagnetization of rocks: analysis of results, in *Methods in Palaeomagnetism,* pp. 254–286, eds Collinson, D.W., Creer, K.M. & Runcorn, S.K., Elsevier, Amsterdam.